

# Development of an invariant display strategy for spectral imagery

J. Scott Tyo<sup>a</sup>, David I. Dierson<sup>a</sup>, and Richard C. Olsen<sup>b</sup>

<sup>a</sup>Electrical and Computer Engineering Department

<sup>b</sup>Physics Department

Naval Postgraduate School

Monterey, CA 93943

## ABSTRACT

There is currently no standard method to map high-dimensional spectral data into a pseudocolor representation. A number of methods have been developed for particular applications, but the results are often difficult to predict when the strategy is applied in other circumstances. A talented analyst can almost always create a color representation that highlights the specific feature of interest, but there is a need for a default strategy which can provide a reliable first look at the data in an unsupervised manner. In this paper, we introduce a principal components based mapping strategy that is built on the principles of human color vision. Orthogonal image information is mapped into orthogonal color processing channels, providing an ergonomic representation that more closely resembles scenes that human visual systems are trained to process. The specific transformation discussed in this paper is optimized for to the data set analyzed, but it provides a first step in the development of an invariant strategy for initial display of spectral data.

**Keywords:** Spectral Imagery, Display Strategies, Colorimetric Representations

## 1. INTRODUCTION

Spectral imagery has emerged as a potentially powerful tool for classifying a scene in remotely sensed images. Many promising strategies for target identification, material classification, terrain mapping, etc., have been developed that take advantage of the information in the hundreds of spectral samples taken at each pixel in a scene. Once a classification algorithm or image processing tool has been applied to a spectral image, the resulting processed data is invariably mapped into a pseudocolor image. While many display methodologies are quite powerful, there is no standard tool used to render spectral imagery in false-color images for presentation.

Currently, the use of false color displays is generally reserved as a tool for presenting data after processing. Once a scene has been classified by a particular algorithm, a specifically tailored colormap is created to emphasize the performance of the classification system. Commonly, in an attempt to distinguish scene elements, one displays the data as an initial processing step, but rarely is visualization in and of itself used as a tool that allows the spectral analyst to perform identification before cueing more powerful processing strategies.

Most colormaps in use today have been developed based on the mathematics of spectral images without considering the workings of the human vision system. It has been demonstrated that failure to consider how the observer processes data visually can make information difficult to find in an image, even when the data are clearly available.<sup>1</sup> This paper represents an attempt to begin incorporating knowledge of human color processing into display strategies for spectral imagery with the goal of developing an invariant strategy for presentation of high-dimensional images.

## 2. FOUNDATIONS OF HUMAN COLOR VISION

It is well known that human color vision is a three-dimensional ( $3 - D$ ) system that operates by sampling the visible spectrum with three photopigments that have maximum sensitivity at approximately 440-nm, 540-nm, and 575-nm.<sup>2</sup> It has also been known for many years that the human vision system processes color by means of an achromatic channel and two opponent-color channels, one which is red-green opponent, one which is blue-yellow opponent.<sup>3</sup> It was demonstrated by Buchsbaum and Gottschalk<sup>4</sup> that the principal components of the spectral sensitivities of

---

Authors' email addresses: tyo@ieee.org, olsen@nps.navy.mil

Presented at *SPIE Imaging Spectrometry VI*, San Diego, August 1, 2000

the three photopigments results in computed channels which are achromatic ( $A$ ), red-green opponent ( $R - G$ ), and blue-yellow opponent ( $B - Y$ ). Their result was the first mathematical explanation for why the human vision system processes color via opponent channels. The opponent colors formulation is used in following sections to develop a display strategy for spectral imagery.

Because the  $A$ ,  $R - G$ , and  $B - Y$  channels are formed from a principal components analysis, they are statistically uncorrelated, and therefore make up orthogonal dimensions in a  $3 - D$  color space. Krauskopf, *et al.*,<sup>5</sup> demonstrated that there are “cardinal directions of color space” - i.e. there are two fundamental axes within color space. There is a  $R - G$  plane where all colors have an absence of yellowness or blueness, there is a  $B - Y$  plane where all colors have an absence of redness or greenness, and the intersection of these two planes is a line with absence of all color. This line is the gray line, and corresponds to the achromatic channel.

The concept of three orthogonal axes has been used to develop the hue, saturation, brightness and the hue, saturation, value (H-S-V) color representation systems. The H-S-V system uses hue to indicate a particular color, e. g. the perceived colors of red, green, blue, etc., saturation to indicate the purity of a particular hue, e. g.  $S = 1$  denotes a pure hue while  $S = 0$  denotes absence of color (gray), and value is related to the brightness or lightness of the particular shade. The perceptual color space therefore makes up a cone, with the  $A$  axis as the axis of the cone and the  $R - G$  and  $B - Y$  axes transverse. Hue is determined by computing an angle in the red-yellow-green-blue plane, and saturation is determined by the angle between a particular point in color space and the gray axis.

An important aspect of the color space is that it is nonlinear, and this is related to the spectral response functions of the individual photoreceptors. As intensity is increased, the hue is perceived to shift, and this is the issue of color constancy.<sup>6</sup> It has also been demonstrated that while red-green and blue-yellow planes exist, other similar color-opponent planes do not seem to exist, hence the term “cardinal directions” used by Krauskopf, *et al.*<sup>5</sup> These subtleties will not be considered in this initial investigation.

### 3. BASIC PSEUDOCOLOR REPRESENTATION STRATEGY

The high-dimensionality associated with spectral imagery at each pixel in a scene is often reduced by means of a principal components (PC) transformation. The PCs are the eigenvectors of the correlation or covariance matrix, and the transformation results in a set of derived variables which are linear combinations of the spectral samples at each pixel. There are several important properties of the PC transformation, including 1) the PCs are orthogonal, i.e. they are statistically uncorrelated (or non-covarying when the covariance matrix is used) within an image and they represent orthogonal directions in  $N - D$  space (where  $N$  is the number of spectral samples at each pixel); 2) each PC corresponds to a nonnegative eigenvalue which gives the fraction of the total variance within the image that projects onto that particular direction in  $N - D$  space; 3) the 1<sup>st</sup>PC (most variance) is guaranteed to be all-positive, and successively higher PCs are expected to have more and more zero-crossings in spectral space.<sup>7</sup> Points 2 and 3 above can be interpreted as follows. The 1<sup>st</sup> principal component has the most variance and therefore is associated with high spatial frequency variations within a scene. In spectral space, the 1<sup>st</sup> principal component is all-positive, and hence is low spectral frequency, i.e. the derived variable does not change rapidly as a function of wavelength. Successively higher PCs are expected to be associated with increasingly lower spatial frequency information (less variance) with more rapid variations in spectral content.

Because of the close similarities between  $N - D$  spectral imagery and  $3 - D$  human color vision, it might be expected that a PC analysis of the two classes of images might provide similar results. This is the case. The  $A$  channel is expected to contain up to 95% of the image variance, and it is a slowly varying function of wavelength with no zero-crossings in the visible spectrum.<sup>4</sup> The  $R - G$  channel has one zero crossing and the  $B - Y$  channel has two zero crossings within the visible spectrum, and they contain the same order of magnitude of the total image variance (2.8% and 1.5% respectively). It was shown by Mullen<sup>8</sup> that the  $A$  channel is most sensitive to high spatial frequency variations within an image, while the  $R - G$  and  $B - Y$  channels act like low-pass spatial filters with similar frequency characteristics. It is demonstrated below that  $N - D$  spectral imagery has very similar properties, and can hence be mapped into the human color perceptual space in an ergonomic fashion.

### 4. CONVENTIONAL COLOR MAPPINGS

The data chosen for initial analysis are from the 1995 AVIRIS overflight of Cuprite Mining District, NV, covering a region that has been used extensively for remote sensing experiments. These data are distributed with ENVI and are

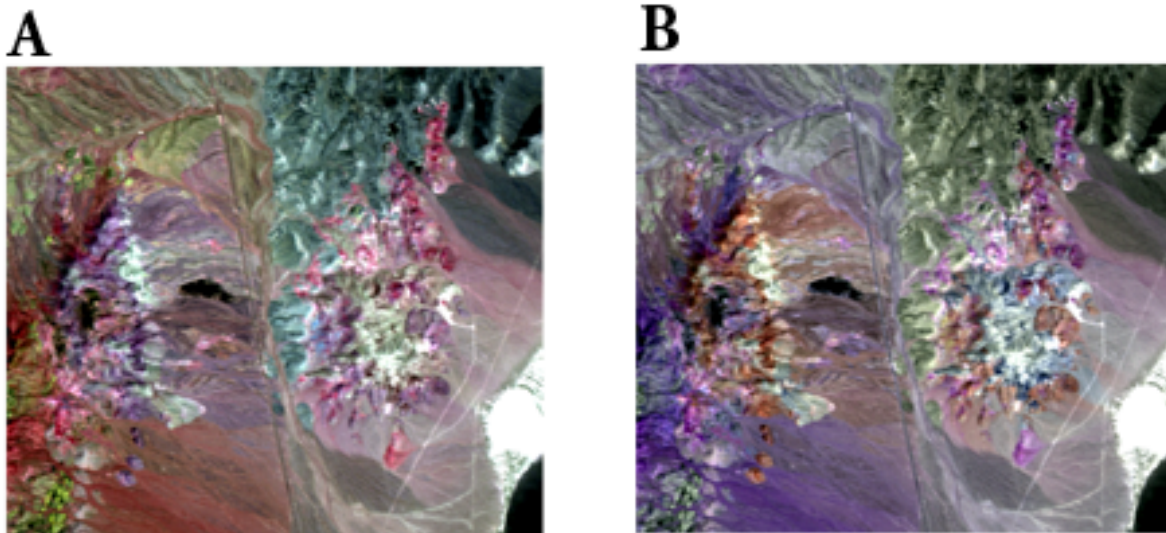


**Figure 1.** Two common mapping strategies for spectral data. A. Three widely spaced bands are chosen in hopes that they are minimally correlated. B. Three particular bands are chosen to highlight a particular spectral feature. It is expected that the mineral kaolinite will appear as magenta, as the green intensity in the RGB image is chosen to lie at the bottom of a kaolinite absorption feature.

used in the ENVI tutorials. They cover 50 contiguous spectral bands from 1.99 to 2.48  $\mu\text{m}$ . All analysis performed here was accomplished using IDL (ver. 5.2.1) and ENVI (ver. 3.2).

Figure 1 presents examples of two popular methods for mapping hyperspectral data into pseudocolor images. In panel A, three widely spaced bands corresponding to  $\lambda = (2.101\mu\text{m}, 2.2008\mu\text{m}, 2.3402\mu\text{m})$  are presented. These bands were chosen because they cover much of the available spectrum, and are likely to be minimally correlated due to their spectral separation. No statistical analysis went into choosing these three wavelengths. Panel B uses  $(R, G, B)$  inputs at  $\lambda = (2.2307\mu\text{m}, 2.2008\mu\text{m}, 2.1309\mu\text{m})$ , wavelengths which were chosen to highlight a particular absorption feature corresponding to the mineral kaolinite, whose representative radiance spectrum is presented in fig. 2.

The two mappings presented in fig. 1 nicely highlight features of the image and segment out regions corresponding to different materials. However, there are many possibilities for choosing the bands corresponding to the  $(R, G, B)$  intensities. The color scheme will change for each of these, and there is not necessarily any *a priori* way to predict the perceived hue for a particular spectral signature. Furthermore, if an individual spectral feature does not overlap with one of the bands chosen for display, that information will not be represented in the final image. For highly specialized mappings like that presented in fig. 1B, it is possible to predict the perceived color for the spectrum that is highlighted, but it is not easy to predict the perceived color of materials with other spectral signatures.

PC analysis offers a potential solution to the problem of seemingly arbitrary choice of bands to map into an  $(R, G, B)$ . The derived variables corresponding to the principal components sample the entire spectral space, therefore it is more likely that prominent spectral features will be included in composing a pseudocolor image using principal components. PC analysis is widely understood, and is described elsewhere.<sup>9</sup> In this study, the covariance matrix is used to derive the principal components. Figure 3 presents the first three principal components of the image. The 1<sup>st</sup> principal component is closely related to the average illumination function, and the eigenvector closely resembles the atmospheric radiance distribution. This is a common occurrence in PC analysis, and it is closely related to the result obtained by Buchsbaum and Gottschalk for human color vision in the visible spectrum.<sup>4</sup> The 2<sup>nd</sup> and 3<sup>rd</sup> PCs each have zero-crossings, but vary reasonably slowly as a function of wavelength.

The normalized eigenvalues obtained by taking

$$\overline{\lambda_i} = \frac{\lambda_i}{\sum_j \lambda_j} \quad (1)$$

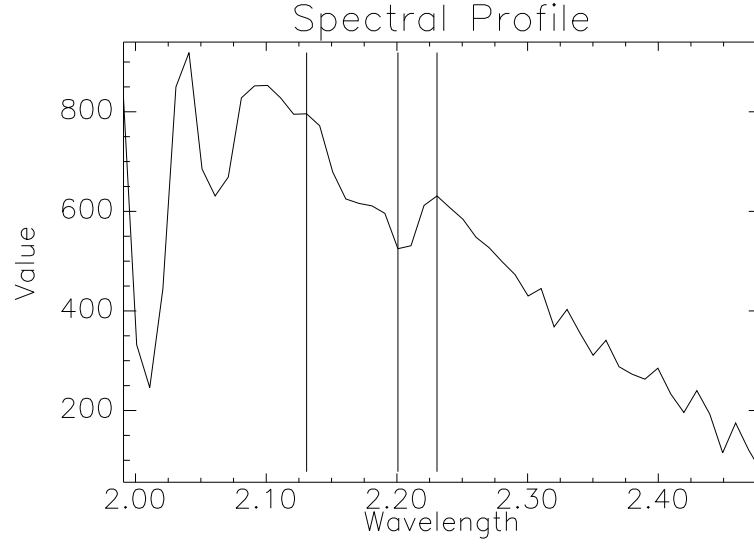


**Figure 2.** Representative spectrum of kaolinite taken from a region in the image known to contain that mineral on the surface. The vertical lines give the spectral locations corresponding to the red, green, and blue intensities in panel B of fig. 1.

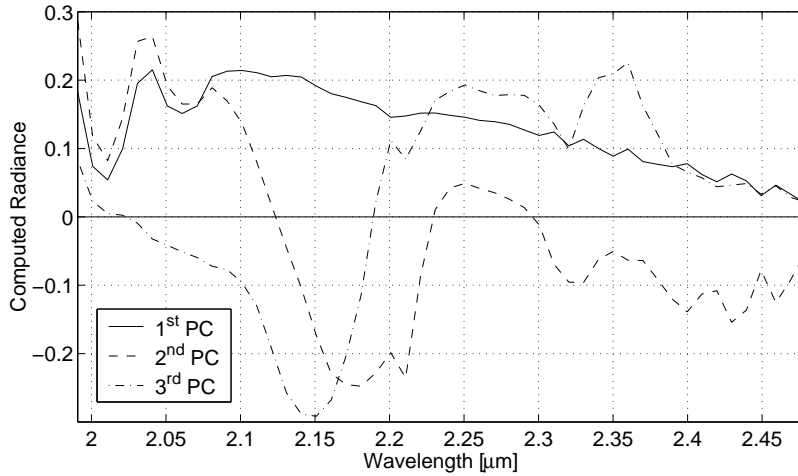


**Figure 3.** First three principal components of the image depicted in fig. 1. Note that the 1<sup>st</sup> principal component is all positive, and the second and third have similar spectral shapes, though they are orthogonal.

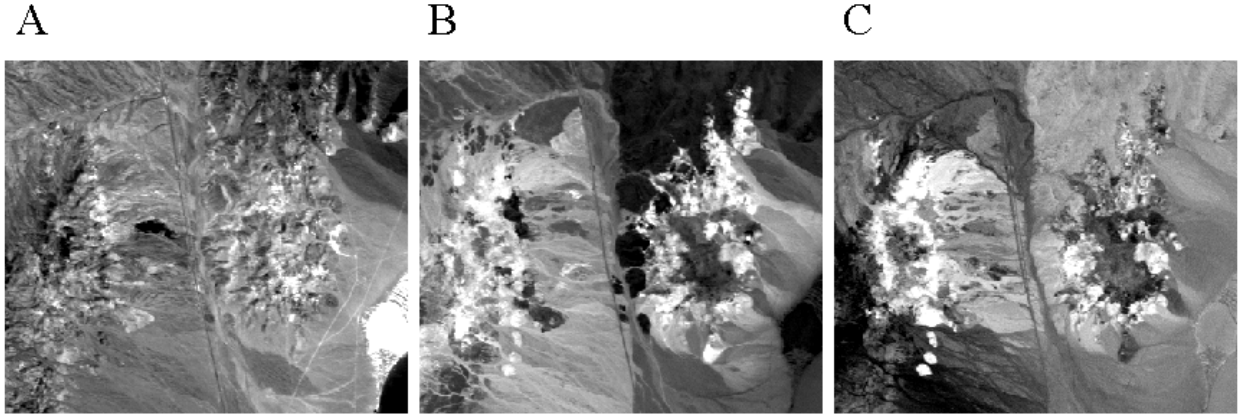


**Figure 4.** First three PC images. The high spatial frequency information corresponding to geography is represented in panel A, while lower spatial frequency information corresponding to classification information is represented in panels B and C. The spatial frequency content of panels B and C are similar, as are the overall spectral shapes of the 2<sup>nd</sup> and 3<sup>rd</sup> PCs.

are  $\lambda_1 = 0.922$ ,  $\lambda_2 = 0.0476$ , and  $\lambda_3 = 0.0233$  (where  $\lambda_i$  represents the  $i^{th}$  eigenvalue, not the wavelength). Summing these eigenvalues indicates that over 99.3% of the variance in the image is contained in the first three PCs. The corresponding PC images obtained by taking the projection of the spectrum at each pixel onto the PC vectors in fig. 3 are presented in fig. 4. Unlike the intensity distribution in any particular band, the PCs provide spectral functions that sample the entire region of interest, preventing any one feature from being completely missed.

A common method for presenting the PC images in a pseudocolor display is to map the first three PCs (or another set of three PCs) into a  $(R, G, B)$  image. An example of such an image is presented in fig. 5A. A second strategy that has been used by us in the past is to map the 2<sup>nd</sup>PC into the  $R$  and  $G$  intensity and the 3<sup>rd</sup>PC into  $B$ . An example of such an image is presented in fig. 5B. The performance of these mappings is discussed and compared in section 6 below.

## 5. OPPONENT COLORS MAPPING STRATEGY

It is clear from the above discussion that there is a close relationship between the nature of the first three PCs in the spectral image being investigated and the corresponding spectral channels in human vision. The 1<sup>st</sup>PC is roughly achromatic, in that it samples the mean illumination distribution. The resulting image contains the high spatial frequency information, as well as the majority of the scene variance. This channel is clearly related to the  $A$  channel in human vision. The second and third PCs have a total of about 7% of the scene variance, and the resulting images contain lower spatial frequency information. The high spatial frequency information in fig. 4A is approximately equivalent to an overall reflectance map, as the 1<sup>st</sup>PC samples the entire spectrum of interest. The images in fig. 4B and C start to present classification information, as regions of like materials tend to group together. These features of the PC images suggest an ergonomic mapping from principal components space to pseudocolor space. The intensity of the 1<sup>st</sup> PC image is mapped into the  $A$  channel, the value of the 2<sup>nd</sup> PC image is mapped into the  $R - G$  channel, and the value of the 3<sup>rd</sup> PC image is mapped into the  $B - Y$  channel. This mapping is almost equivalent to the following strategy:

$$\begin{aligned} \phi &= \text{atan} \left( \frac{P_3}{P_2} \right) && \rightarrow H \\ \frac{\sqrt{P_2^2 + P_3^2}}{P_1} &&& \rightarrow S \\ P_1 &&& \rightarrow V \end{aligned} \quad (2)$$

where  $H$ ,  $S$ , and  $V$  are hue, saturation, and value, and  $P_i$  is the  $i^{th}$  PC. The mapping in (2) is not exactly correct because hues that are separated by  $180^\circ$  are not typically perceived as being exactly opponent, and some reshaping of the color space is necessary, as shown in fig. 6.

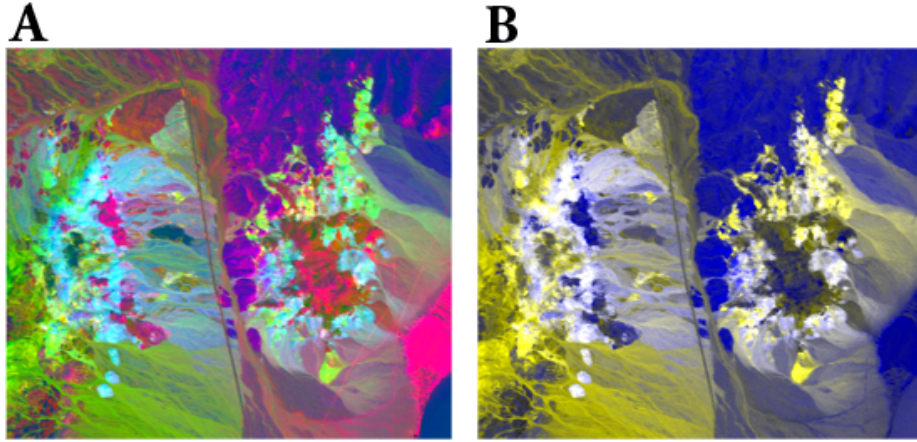


**Figure 5.** Pseudocolor representations obtained by mapping A. First three PCs into  $(R, G, B)$ . B. Second PC into the red and green, third PC into blue.

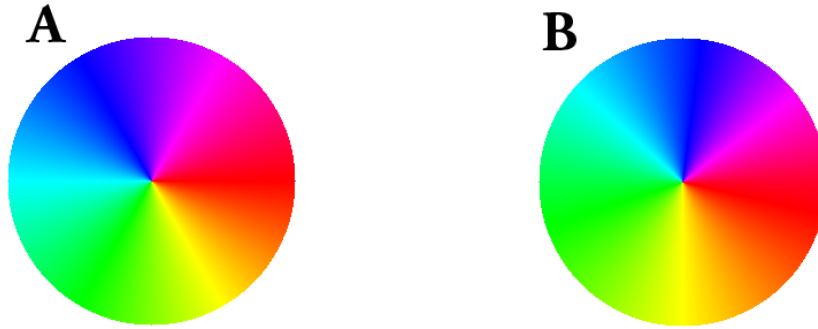


**Figure 6.** Hue wheels using the default (panel A) and reshaped (panel B) values of hue.

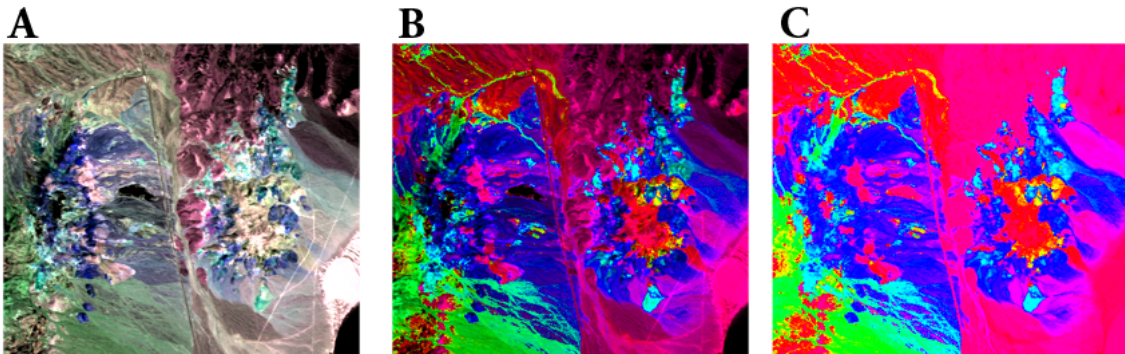


**Figure 7.** Three mappings which send the principal components into the  $(H, S, V)$  color space. A. Full implementation of (2) with saturation amplified so that the maximum value of  $S$  in the image is 1. B. Suppression of saturation. Each pixel is fully saturated, but the 1<sup>st</sup> and third equations in (2) are still employed. C. Only the hue is mapped

Figure 6A has a wheel that is composed using the default hue selections for Matlab, while fig. 6B has been reshaped to make the colors red, blue, green, and yellow correspond to the angles  $0^\circ$ ,  $90^\circ$ ,  $180^\circ$ , and  $270^\circ$ , respectively (as perceived by the authors).\*

Once the mapping described by (2) is accomplished, there are still several choices available to the user. Figure 7A presents the full mapping, with the value of  $S$  stretched so that the maximum saturation in the image is 1, corresponding to a stretching factor of 2.3. This image nicely represents all of the information in the three PC images of fig. 4 in a manner that is readily interpreted by the observer. The geographical information (high spatial frequency) is maintained in the  $A$  channel, while the classification information from  $P_2$  and  $P_3$  is mapped into color. While there are clearly pixels that are highly saturated (after stretching), many pixels in the image have low saturations, as these pixels have small projections on the  $P_2 - P_3$  plane. A second possible mapping involves the suppression of saturation information. This method, shown in fig. 7B, presents each pixel as fully saturated (pure hue), and results in a “closest classification” image, i. e. each pixel is assigned to the material (hue) that it most closely resembles. Similar strategies are often employed for display when using an endmember selection strategy.<sup>10</sup> However, by superimposing the intensity information from  $P_1$ , the geographical features can more clearly be seen. The third possible mapping, presented in fig. 7C, involves suppression of both saturation and value, and results in a typical classification image where each pixel is assigned to the material (hue) that it matches most closely with  $S = 1$  and approximately constant intensity ( $V = 0.75$  in fig. 7C).

## 6. DISCUSSION

In the preceeding sections, several mapping strategies were presented for displaying high-dimensional spectral data in a scene. A brief discussion of the relative merits of each method is presented here. The class of mappings presented in fig. 1 is possibly the most powerful set of methods. When a particular spectral feature is to be highlighted, a particular material uncovered, etc., then a specifically tailored color mapping strategy should be developed. Numerous examples of such strategies have appeared in the literature. The images in fig. 1 nicely present the high spatial frequency information that depicts the geography. This is expected because areas that have uniformly low reflectance will be dark in all three bands, and therefore dark in the final image. The high spatial frequency has therefore been mapped into the  $A$  channel as is desirable. The problem with these strategies is that it is not easy to predice *a priori* the effect of the mapping on the elements of the scene that are *not* being emphasized. Simple mapping of spectral bands into  $(R, G, B)$  space can overlook important spectral features, and different implementations will result in different hues in the final image.

The typical class of PC-based pseudocolor representations depicted in fig. 5 solves the problem of using isolated spectral information, but does not take advantage of the known information about human vision presented in section 2. The PC transformation nicely separates the information into orthogonal variables, but the mappings used in fig. 5 take this orthogonal information and present it in non-orthogonal visual pathways. While some of the high spatial frequency information is apparent in fig. 5A, much of it is suppressed, and there is apparent smearing, which is an artifact of how the viewer *perceives* the data. The mapping in fig. 5B is more ergonomic, but instead of mapping the information into orthogonal channels, the 2<sup>nd</sup> and 3<sup>rd</sup> PCs are mapped into the  $A - (B - Y)$  plane.

The image in fig. 7A has one very important property that makes it easier to view, as compared with images like those in fig. 4A or in ref. 10. Pixels that don’t have a significant projection onto either  $P_2$  or  $P_3$  appear largely desaturated. This makes the image easier to view because naturally occurring scenes tend to be largely desaturated with low dimensionalities in the visible portion of the spectrum.<sup>4</sup> Human observers are not used to examining images with large regions of highly saturated hues that vary rapidly. The set of images in fig. 7 provides a way to go back and forth between highly saturated and less saturated images to make material classification more obvious.

The class of mappings presented in fig. 7 was designed with the performance of the human visual system in mind. It is also closely related to one of the common processing strategies in spectral imagery, namely the representation of scatterplots. Scatterplots are projections of high-dimensional spectral data onto a particular  $2 - D$  plane. Usually, the axes are orthogonal dimensions derived from a PC or minimum noise fraction (MNF) transformation. Pixels that are similar project to the same general location in the scatterplot, and if they can be recognized as a distinct

---

\*The mapping discussed here has been optimized for display on an electronic monitor. Different primary hues are used for printing, and no attempt has been made to optimize for those. The images presented in this paper contain most of the desired information, but interested readers are encouraged to contact the authors to obtain an electronic copy of the article in order to see the optimized images on a monitor.



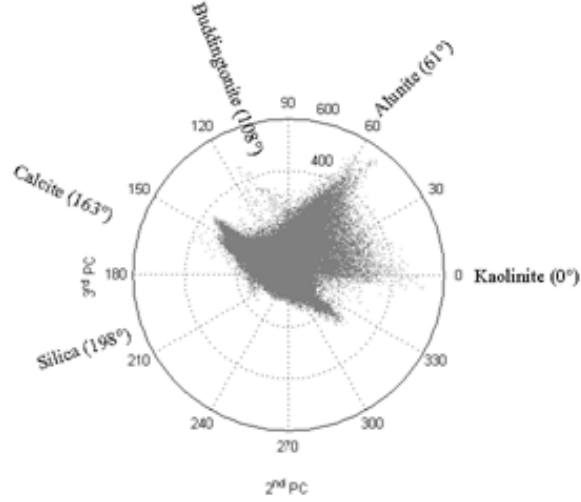


**Figure 8.** Scatterplot projecting each pixel in the image onto the  $P_2 - P_3$  plane. Each direction within this plane corresponds to a specific hue, which can be obtained by comparing the angles in this figure to the angular location of hues in fig. 6. It is apparent in this figure that the approximate origin is close the the point from which the various arms radiate, but more detailed investigation might be merited to determine the exact location of the origin, similar to that performed for the Tasselled Cap Transform for use with LANDSAT data<sup>11</sup>

group, classification can be performed. The scatterplot corresponding to the images presented in fig. 7 is shown in fig. 8. A number of pixels have been identified from gound-truth observations as containing specific materials. A set of regions of interest corresponding to regions of silica, alunite, kaolinite, buddingtonite, and calcite is distributed with the ENVI tutorials. The mean spectrum in each of these regions is presented in fig. 9. The mean solar radiance dominates each of these plots. To find the region of the scatterplot of fig. 8 corresponding to each of these mean spectra, a projection is taken on the first three PCs. The residual spectra obtained by

$$L(\lambda)_{resid} = L(\lambda) - L(\lambda) \cdot P_1 \quad (3)$$

is also shown for each material. It is clear that the classification information is held in the residual spectrum. For each of the five materials, an angle in the  $P_2 - P_3$  plane was computed by taking the appropriate projections, and the results are summarized in table 1. The angular location of each of the materials is also indicated in the scatterplot of fig. 8.

Material	$L \cdot P_1$	$L \cdot P_2$	$L \cdot P_3$	Angle
Silica	4012	-126	-40.6	198°
Alunite	3810	139	253	61.2°
Kaolinite	4063	264	1.92	0.415°
Buddingtonite	3980	-109	337	108°
Calcite	4988	-187	57.2	163°

**Table 1.** Projection of the mean material spectra on the first three PCs, as well as angle in the  $P_2 - P_3$  plane as indicated in the scatterplot of fig. 8.



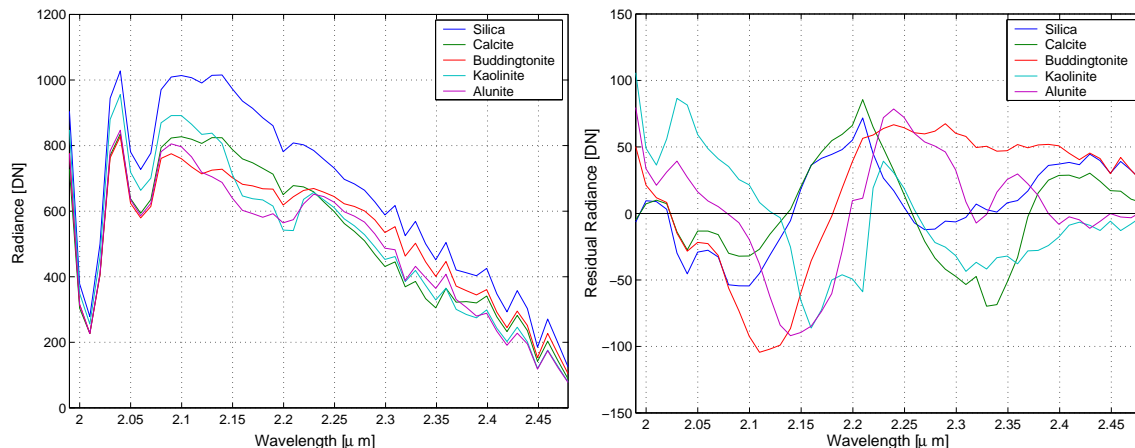


**Figure 9.** Five different material mean spectra obtained by averaging over a ground-truthed region of the data. A. Mean spectrum. B. Residual remaining after subtracting the projection of the mean spectrum onto the 1<sup>st</sup> PC shown in fig. 3

## 7. CONCLUSIONS AND FUTURE DIRECTIONS

The principal component-based mapping strategy discussed here provides an easy way to perform first order unsupervised classification. The resulting image is segmented spatially based on the projection of the local radiance distribution in the  $P_2 - P_3$  plane. By visually inspecting the resulting image, the analyst can the direct attention to appropriate areas of the scene for further processing.

There is an important aspect of the PC processing that should be mentioned. The ENVI software package automatically rescales the PC rotation so that the geometric mean of the data is located at the origin of the transformed space. The amount of translation varies for each PC axis, and to the best knowledge of the authors, there is no way to extract the shifts from the statistics file. For that reason, all PC images were computed manually in IDL by projecting the pixel spectra directly onto the corresponding eigenvectors. This is extremely important, as translating intensities is equivalent to moving the origin in the  $P_2 - P_3$  plane, which is in general not desired. Shifting the origin will cause a line which is supposed to travel radially outward from the origin to cover a range of angles, introducing hue shift as a function of intensity.

The PC transformation presented here was derived specifically for the data set in the images. The question still remains as to whether a general set of PCs can be derived that is broadly applicable to classes of spectral imagery. It is expected that the 1<sup>st</sup> PC will always be related to the mean solar radiance (which is predictable), but the 2<sup>nd</sup> and 3<sup>rd</sup> PCs will depend on the specific contents of the image. If a set of general PCs can be identified, the color mapping can be arranged so that materials are presented in a straightforward manner, i.e. water can always be mapped to blue, etc. Also, as a wider range of wavelengths is considered, it should be expected that more than 3 PCs will be necessary to capture an equivalent amount of the data (99% or more).

The presentation strategy discussed here is best suited to geographical classification, not for identifying small, isolated targets. Targets which occur only at a few pixels in an image will have little effect on the overall covariance matrix, and will not contribute significantly to the 2<sup>nd</sup> and 3<sup>rd</sup> PCs. For this reason, such small targets *may* have small projections in the  $P_2 - P_3$  plane. This is a subject that merits significant investigation.

The pseudocolor mapping strategy presented here is offered as a way to take a first look at the data. By performing an unsupervised PC transformation and analyzing the most significant PCs, initial classification decisions can be made. Better yet, if an invariant strategy is developed, the scene can be mapped to a standard color representation that allows ready interpretation. It is important to compare the PC eigenvectors that result in classes of images in order to determine if a standard transformation can be applied for particular remote sensing tasks, similar to the Tasseled Cap Transform<sup>11</sup> developed for multispectral LANDSAT sensing of agricultural targets. Detailed investigation of the relationship between the PC eigenvectors and image content is needed to determine how robust

the strategy is. Comparison with other classification strategies is merited in order to quantify the usefulness of this presentation strategy in general.

## REFERENCES

1. J. S. Tyo, E. N. Pugh, Jr., and N. Engheta "Colorimetric Representations For Use With Polarization-Difference Imaging Of Objects In Scattering Media" *J. Opt. Soc. Am. A* **15** pp. 367-374 (1998)
2. J. J. Vos and P. L. Walraven, "On the derivation of the foveal receptor primaries" *Vision Res.* **11** pp. 799-818 (1971)
3. See for example G. Wyszecki and W. S. Stiles, *Color Science* (Wiley, New York, 1967)
4. G. Buchsbaum and A. Gottschalk "Trichromacy, Opponent Colours Coding And Optimum Colour Information Transmission In The Retina" *Proc. R. Soc. Lond. B* **220** pp. 89-113 (1983)
5. J. Krauskopf, D. R. Williams, and D. W. Heeley, "Cardinal Directions of Color Space" *Vision Res.* **22** pp. 1123-1131 (1982)
6. D. H. Brainard, B. A. Wandell, and E.-J. Chichilnisky, "Color Constancy: From Physics to Appearance" *Current Directions in Psychological Science* **2**(5) pp. 165-170 (October 1993)
7. A. Bermann and R. J. Plemmons, *Nonnegative Matrices In The Mathematical Sciences* Chapter 4 (Academic Press, New York, 1979)
8. K. T. Mullen, "The Contrast Sensitivity Of Human Colour Vision To Red-Green And Blue-Yellow Chromatic Gratings" *J. Physiol. (London)* **359** pp. 381-400 (1985)
9. H. L. van Trees, *Detection, Estimation, and Modulation Theory* Part I (Wiley, New York, 1968)
10. M. E. Winter, "Fast autonomous spectral endmember determination in hyperspectral data" 13<sup>th</sup> *International Conference on Applied Geologic Remote Sensing* Vancouver, BC, Canada March 1999
11. R. J. Kauth and G. S. Thomas, "The tasselled cap – a graphical description of the spectral-temporal development of agricultural crops as seen by LANDSAT" *Proceedings of the Symposium on Machine Processing of Remotely Sensed Data* pp. 4B41-4B51 (Purdue University, West LaFayette, IN, 1976)